Credit: 2 PDH

Course Title:

Recent Development in Aquaporin Membrane Design

Approved for Credit in All 50 States

Visit epdhonline.com for state specific information including Ohio's required timing feature.

3 Easy Steps to Complete the Course:

1. Read the Course PDF
2. Purchase the Course Online & Take the Final Exam
3. Print Your Certificate

Chapter 7

Recent Development in Aquaporin (AQP) Membrane Design

Amira Abdelrasoul, Huu Doan and Ali Lohi

Additional information is available at the end of the chapter

http://dx.doi.org/10.5772/intechopen.71724

Abstract

Development of Aquaporin Z (AqpZ) proteopolymersome has been substantial enough that it can obtain water separation membranes that feature fluxes of 11,000 L m^{-2} h^{-1}, a parameter value that is multiple orders of magnitude greater than the conventional industrial membranes available and possible only if the performance of AqpZ proteopolymersome can be properly scaled up. In fact, densely packed 2D AqpZ crystal arrays can in theory reach flux capacity of up to 16,000 L m^{-2} h^{-1}. On the other hand, these flux values may likely not be reached in practice, since various upscaling issues would prevent them from occurring. Nonetheless, AqpZ offers immense potentials benefits when it comes to biomimetic membranes. The research in membrane development is continuously ongoing, for example, only a few years ago in 2011, aquaporin-based biomimetic polymeric membranes (ABPMs) were viewed as the radically advanced membrane solution and, at the same time, removed from practical applications and commercial production. After 4 years of innovative thinking, ABPM membranes are produced for commercial consumption and with area dimensions of tens of m^2. Although it will take some time before this membrane technology becomes universally accessible, it has already gone beyond the confines of research theory and into practical application. The following chapter will explicitly outline the development of AQP biomimetic membrane technology.

Keywords: Aquaporin Z, membrane design, biomimetic structures, interfacial polymerization

1. Introduction

Development of Aquaporin Z (AqpZ) proteopolymersome has been substantial enough that it can obtain water separation membranes that feature fluxes of 11,000 L m^{-2} h^{-1}, a parameter value that is multiple orders of magnitude greater than the conventional industrial membranes

available and possible only if the performance of AqpZ proteopolymersome can be properly scaled up. In fact, densely packed 2D AqpZ crystal arrays can in theory reach flux capacity of up to 16,000 L m^{-2} h^{-1} [1]. On the other hand, these flux values may likely not be reached in practice, since various upscaling issues would prevent them from occurring. Nonetheless, AqpZ offers immense potentials benefits when it comes to biomimetic membranes. The research in membrane development is continuously ongoing, for example, only a few years ago in 2011, aquaporin-based biomimetic polymeric membranes (ABPMs) were viewed as the radically advanced membrane solution and at the same time far removed from practical applications and commercial production [2]. After 4 years of innovative thinking, ABPM membranes are produced for commercial consumption and with area dimensions of tens of m^2 [3]. Although it will take some time before this membrane technology becomes universally accessible, it has already gone beyond the confines of research theory and into practical application. The following sections will explicitly outline the development of AQP biomimetic membrane technology and the research that helped to produce.

2. Planar biomimetic structures and membrane designs

The early industrial application approaches to membrane design were released by two Danish companies. They are the AquaZ (now Applied Biomimetic) and Aquaporin A/S. With the collaboration of the Danish Technical University (DTU), the University of Southern Denmark (SDU), DHI, Lund University in Sweden, Malaga University in Spain, Vilnius University in Lithuania, Ben-Gurion University of the Negev in Israel, and Veolia Water in France, the Aquaporin A/S joint research group became part of the EU-funded MEMBAQ project from 2006 to 2010, where they explored ways of using AQPs in industrial applications [4]. During the same period, AquaZ began to research on membrane development framed by the patent from Carlo Montemagno. In this patent, Montemagno conceptually outlined how AQPs that are embedded in lipid or polymeric bilayers can in theory function as a type of biomimetic membrane, despite offering a distinct design for the membrane [5].

The original Aquaporin A/S membrane design was constructed around the idea of an ethylene tetrafluoroethylene (ETFE) scaffold with 300 μm holes, created using laser-ablation, and directly inspired by the practice of painting or folding lipid chambers begun in the 1970s [6, 7]. In its earlier form, a freestanding lipid-bilayer film was created through the process of "painting" a two-phase solution over the area of the hole, specifically in places where the lipids transform from the organic solvent phase to the aqueous phase and then collect around the openings to form the bridging layers. A number of membrane peptides and proteins were integrated into the freestanding layers, such as porins [8]. Furthermore, freestanding polymethyloxazoline-polydimethylsiloxane-polymethyloxazoline (PMOXA-PDMS-PMOXA) polymer membranes with integrated gramicidin A channels were created [9] and then comprehensively categorized [10]. In the designs that followed, the membrane is maintained by PEO-dimethacrylate (PEO-DMA) type of hydrogels [11] or stabilized with the aid of surface plasma polymerization process [12]. In addition, an approach that was formulated during the continuous oil phase would create an interface lipid bilayer in between the lipid-coated

water drops [13]. A later iteration of membrane design examined liquid membrane method with relatively small water flux for Spinach plasma membrane protein 2;1 (SoPIP2;1) proteoliposomes, which was placed between the NF membranes that were capable of providing an AQP fingerprint [14]. Designs such as these [14–18] helped to encourage innovative approaches to membranes and develop membrane-based biosensor projects [19]. In 2010, the hydrogel method created at Aquaporin A/S was introduced. This occurred once AquaZ and Montemagno came out with the ABLM design that featured internally cross-linked UV and PA-interconnected proteoliposomes that are positioned as motionless on the lipid-coated PA layer and maintained with a PEO hydrogel [20].

DHI Singapore and Aquaporin A/S began research collaboration with the SMTC on biomimetic membranes and their applications in 2009. Simultaneously, the Chung lab at NUS initiated biomimetic research project in conjunction with Wolfgang Meier research group. The collaboration at NUS continued to examine the Aquaporin's hydrogel method and attempted to create a planar proteobilayer, beginning with AqpZ proteoliposome fusion process conducted with pure and PEO-coated porous alumina. During the experimental runs, the research team recognized an increase in stability as the mPAR values became greater [21]. This method was outlined in 2012 as relying on a Langmuir-Blodgett film with nickel-chelated lipids that effectually binds to the histagged AqpZ. This method is similar in its framework to the approach developed by Kumar [22], however, based on lipids with consequent Langmuir-Schäffer deposition-mediated transfer onto the mica surface [23]. Kaufman et al. attempted to further the research by integrating spinach AQP (SoPIP2;1) into the positively charged bolalipid micelles that were fused on the negatively charged silica surface [24]. Research conducted by Tang et al. examined proteoliposomes fusion performance on polymer-coated and pure silica with the help of quartz crystal microbalance with dissipation (QCM-D) [25]. Tang et al. identified higher robustness as well as fusion resistance capabilities as the mPAR increased and additional proteoliposome stabilization potential with polyelectrolyte layers functioning at the maximum mPAR (1:25) in 1,2-diphytanoyl-sn-glycero-3-phosphocholine (DPhPC) liposomes [25]. SMTC research group likewise examined ABLMs in an attempt to further Kaufman's method for liposome fusion process on nanofiltration (NF) membranes, [26, 27] and fused AqpZ proteoliposomes on NF PA-polysulfone (PSf) membranes intentionally precoated with positively charged lipids using the spin-coating process [28]. In this case, the proteoliposomes were positioned onto the NF membrane and then slightly pressurized with 0.5 bar. The data obtained indicate that a linear correlation between the ABLM surface's roughness quality and mPAR shows AqpZ integration; however, an observable absence of influence from AqpZ onto the water flux Jv or the reverse salt flux J_s [28] was found.

3. Vesicular biomimetic structures in membrane design

Aquaporin A/S and SMTC launched a joint collaborative approach where AqpZ proteoliposomes were effectively inserted in the standard PA layer created using interfacial polymerization of trimesoyl chloride (TMC) and *m*-phenyl diamine (MPD) on a PSf support structure [29–31]. In this case, ABLMs were verified through testing with functional AqpZ proteoliposomes, PA-PSf

membranes without any proteoliposomes, and proteoliposomes that include an inactive AqpZ mutation. The ABLMs and their qualifications were rigorously compared to the commercially available membranes with the aid of cross-flow RO tests on 42 cm^2 effective area. Although the *Js* values were similar in all the cases, the ABLMs including AqpZ proteoliposomes showed substantially higher *Jv* values than those measured for the ABLM with inactive AqpZ and PA-PSf membranes. Moreover, the ABLMs were capable of enduring 10 bar pressure, thus identifying them as suitable for applications with low-pressure RO. The ABLM *Jv* values were ~40% greater when compared to the commercially available brackish water RO membranes (BW30), as well as an order of magnitude higher if compared to the seawater RO membranes (SW30HR). The results of this analysis were further advanced through a systematic study showing that 1,2-dioleoyl-sn-glycero-3-phosphocholine (DOPC)–based proteoliposomes and proteoliposomes with mPAR of 1:200 offered the ideal water flux values as suggested by SFLS. The study also indicated that the addition of cholesterol might be able to seal the defects occurring on the proteoliposomes [32].

In order to obtain better sealing parameters and higher loading capacity, the SMTC research group tried to coat proteoliposomes with polydopamine (PDA) and then immobilized them on a 28-cm^2 NF polyamide imide (PAI) membrane by inserting them into the branched polyethyleneimine (PEI) that was crosslinked per PA bond at higher temperature values [33]. The data collected by SFLS indicated that the increased temperature values had greater adverse effects on the proteoliposomes' permeability potential than the PDA coating. Despite the potential issues, AqpZ functionality was shown and validated with optimized performance mPAR values of 1:200 once included and reconstituted into the PAI-PEI layer. Alternatively, the maximum SFLS results were reached at an mPAR value of 1:100 [32]. The reasons for this difference could be connected to the fact that AqpZ is influenced by the PEI branches or the PDA coating. Nevertheless, the *Jv* value was calculated as 36 L m^{-2} h^{-1} bar^{-1}, a result that qualifies it as the most advanced in all currently available biomimetic membranes [33].

Proteopolymersomes can also be further functionalized during the process of getting chemically bounded to a functional membrane counterpart. The process of liposomes and polymersomes functionalization has been widely researched for a number of decades [34–36]. The ABPMs featuring functionalized proteopolymersomes were originally introduced in a 2011 Montemagno patent. This patent established the conceptual framework for proteopolymersomes created out of polyethyloxazoline-polydimethylsiloxane-polyethyloxazoline (PEOXA-PDMS-PEOXA) triblock copolymers. In this type of proteopolymersomes, the methacrylate-functionalized PEOXA block is restraining the proteopolymersomes on a methacrylate functionalized cellulosic membrane [37]. After the patent was finalized, the initial experimental results collected during a practical application of this method were given by the NUS group [38]. This research group manufactured proteopolymersomes including AqpZ in methacrylate-functionalized PMOXA-PDMS-PMOXA and then tested them using SFLS. Unlike the data collected by Kumar and researchers [39], there were no substantial changes in SFLS signals when alternating mPAR values, a dynamic that reflects the potential concerns that exist with SFLS when it comes to rigid structures. Montemagno et al. reported that the proteopolymersomes were placed onto the acrylate-functionalized polycarbonate track-etched (PCTE) membranes and then immobilized using UV-crosslinking of the acrylate

groups and implementing methacrylate of the PMOXA [37]. After this procedure, the proteopolymersomes were restrained even more through the process of pressure-assisted adsorption and potentially shattered using the "smooth extrusion". The AQP caused an augmentation in the *Jv* values as the mPAR values became higher, while there was an absence of *Jv*, when the polymersomes were applied by themselves. On the other hand, field emission-scanning electron microscopy (FE-SEM) and AFM exposed that the layer had a number of defects or imperfections [38]. In a research study conducted soon after, Montemagno et al. emulated a similar method that relied on acrylate-functionalized cellulose acetate membranes [40]. In this experimental dynamic, the researchers saw a surge in *Jv* values and a reduction in NaCl rejection potential with proteopolymersomes that have larger mPAR values. The marked growth in *Jv* values may be a sign of AQP activity; however, the NaCl rejection remained relatively low (33%) and the determined membrane area was quite small at only 7 mm^2 [40].

A different method suggested gold-disulfide binding for immobilization of disulfide-functionalized PMOXA-PDMS-PMOXA AqpZ proteopolymersomes on silicon and gold-coated porous alumina surfaces [41]. This FE-SEM approach indicated that complete pore coverage was attained at the pore diameter of 55 nm, and where greater size pores of 100-nm diameter continued to be open. As a result, despite observing the integration of AQP, the NaCl rejection potential was small [41]. In order to achieve an improved sealing capacity, the cysteamine was introduced with PDA as well as histidine coatings, once the proteopolymersome immobilization process on gold-coated PCTE was done [42]. The experimental data suggested that the *Jv* values increased, while the *Js* values decreased, as number of PDA-His layers increased. On the other hand, the ideal sealing capacity was achieved without the use of the proteopolymersomes. The pressure-reversed osmosis (PRO) mode testing (AL toward the water receiving draw side) caused a substantially higher *Js* values than the forward osmosis (FO) method of testing (AL toward the feed side) [42]. The mathematical simulations used for the ABPM suggest that when using the PRO mode, *Jv* value is dictated by permeability potential and the size of the vesicle. Alternatively, when applying the FO mode, the hydrostatic pressure value is shaped by the vesicle interior's solute concentration [43].

Innovation in membrane research helped initiate another variation of the method design that has been developed experimentally using AqpZ and methacrylate-functionalized and carboxyl-functionalized PMOXA-PDMS-PMOXA with amine-functionalized CA [44]. In this method, the proteopolymersomes are initially covalently connected to the CA, where the amine groups on CA and the carboxyl groups of PMOXA develop a PA bond. The approach then relies on the methacrylic cross-linking polymerization that is achieved by dipping the membrane into a mixture of ethylene glycol dimethacrylate, methyl methacrylate, and an initiator. As the polymerization time increases, the *Jv* value is linearly growing, while the NaCl rejection potential is reducing. A growth in *Jv* values and a drop in NaCl rejection of ABPMs were comparable to only polymersome-coated CA and methacrylated CA in both NF and FO modes and showed existence of AQP. Alternatively, the NaCl rejection rate of 61% suggested major defects and imperfections [44]. Additional illustration of methacrylate cross-linking is based on amine-functionalized AqpZ proteoliposomes with a PDA-precoated ultrafiltration (UF) polyacrylonitrile (PAN) membrane [45]. In this instance, the proteoliposomes are cross-linked internally using methacrylate and then slowly pressurized onto the PDA-PAN support, thus

permitting the response of functionalized lipids and PDA amines. Additional stabilization is obtained with the aid of glutaraldehyde. The process of internal proteoliposomes cross-linking had a helpful influence on the overall stability. *Jv* and NaCl rejection potential between ABLMs and liposome-coated membranes indicated some effects that signal the presence of AqpZ. The low NaCl rejections and FE-SEM images reflected that the imperfections in the ABLM had a serious role in the membrane's performance [45]. Rather than rely on the process of chemical bonding, proteoliposomes or polymersomes have the capacity to be bound together by electrostatic forces. Kaufman et al. tried to use this approach so as to fuse positively charged bolamphiphilic proteoliposomes onto negatively charged NF PA and with sulfonate PSf (PSS) membranes [46]. In this experimental setup, the proteoliposome loading was improved due to the more negatively charged PSS membrane. The proteoliposome loading likewise contributed to a decrease in *Jv* values in addition to a raise in NaCl rejection potential, primarily because of the produced defects within the bolamphiphilic bilayer by SoPIP2;1 [46].

As researchers continued to expand alternative approaches, an electrostatic-binding-based approach was created and it relied on the process of embedding positively charged poly-L-lysine covered AqpZ proteoliposomes into the anionic section of a layer-by-layer (LbL) sandwich on a UF PAN membrane [47]. In this method, the anionic section consists of polyacrylic acid (PAA) and PSS and where the cationic counterpart is created out of the polyallylamine hydrochloride (PAH). When this method was applied experimentally, a distinct AqpZ effect was seen, *Jv* values were raised by 30–50% after the proteoliposomes addition, and the overall effect was greater once there were a larger number of negatively charged lipids available. In this experimental setup, the $MgCl_2$ rejection rate was comparable to the results obtained in the research data collected by Zhao et al. [29], but notably, there was no NaCl rejection available [47]. This research approach was further elaborated by encapsulating magnetic nanoparticles to incite more proteoliposomes to magnetically adsorb the polyanionic film. In this type of FO mode, the measured data showed a raise in *Jv* as well as *Js* values as the mPAR increase, and this accounts for the residual flaws, despite the attempts to introduce more vesicles onto the supporting substrate [48].

Together with other researchers from Ocean University in China, Wang continued to develop the earlier methods. In particular, they were able to immobilize AqpZ proteoliposomes using positively charged lipids on top of a negatively charged PSS layer, which was then followed by PEI on an UF PAN membrane [49]. Once the experimental data were collected, it became clear that the modest NaCl rejection capacity and *Jv* decrease suggest a highly imperfect membrane. A growth in *Jv* occurring between proteoliposomes and liposomes, in addition to an increase in *Jv* with greater mPAR values, may be indicative of the AQP presence. In this case, NaCl rejection continued to be unchanged for all membranes. The membrane performance was shown to be compromised, when the detergent treatment was used [49].

The method designs are comprehensively summarized [49], and the research data collected help to conclude that the embedment of proteopolymersomes or liposomes in a layer facilitates significantly more efficient membranes, if compared to layer-based immobilization approaches. One of the key benefits of the PA-embedment technique is that there is no need to precoat or functionalize processes that can severely limit any potential for upscaling and large

applications [29]. The described performance data are relatively inefficient when compared to the theoretical predictions, since much more innovation is necessary. A critical setback is the fact that with an increasing mPAR values, *Jv* is likewise augmented; however, at the same time, the matrix layer becomes weaker in its structure and thus more susceptible to salt leakage. The inclusion of stabilizing and sealing polymer networks may help the rejection potential, but it might likewise compromise J_v [1]. In addition to ABPMs and ABLMs, two primary research directions are aimed at obtaining functioning biomimetic membranes with the aid of AQP-mimicking artificial channels, specifically organic building block nanochannels and carbon nanotubes (CNTs) [50]. The CNT method is used more frequently due to the fact that its faster water permeation has been proven in theoretical terms [51] as well as experimentally [52]. When it comes to the organic nanochannels and their applicability, five structures have been found promising as they can effectively compete with ABPMs, CNTs, and ABLMs. These five structures include zwitterionic coordination polymers based on zinc and N,N-diacetic acid imidazolium bromide [53], imidazole compounds with urea ribbons [54], helical pores of dendritic dipeptides [55], macrocycles of m-phenylene ethynylene [56], and hydrazine-appended pillar arenes [57]. When it comes to these structures, their primary benefit, if compared to other designs, is a smaller size featuring channel diameter values (3–10 Å) [50].

4. POSS: a new element in interfacial polymerization

Most of the FO and RO membranes are polyamide (PA-based) and are frequently referenced as the thin film composite (TFC) membranes because of their comparatively improved membrane design performance. The PA layer for these types of membranes primarily created using a reaction between an acyl chloride and an amine [58]. For this reaction to occur, there needs to be a process that effectively dissolves the amine group during the aqueous phase, as well as a process that dissolves the acyl chloride group during the organic phase [59]. In most cases, the membrane is fully wetted in the aqueous phase, which includes the amine group. After this initial process, the membrane becomes somewhat dry once the excessive visible liquid is removed, and the surface is kept as moist. In the next step, the organic phase featuring the acyl chloride group is introduced on the surface top area. It can be argued that the reaction's growth is directed into the organic phase [60] because of the preferential solubility that exists in amine group during the organic phase, if compared to the acyl chloride solubility values during the aqueous phase. In this experimental setup, the reaction growth causes the well-recognized valley and ridge formation in the PA layer. The standardized amine-acyl chloride grouping is Trimesoyl chloride (TMC) and *m*-phenyl diamine (MPD), and usually, they are complemented with molecules or additives with analogous chemistries and parameters in lower concentrations so as to improve chlorine resistance, rejection, or flux [58].

For the PA membrane, the ideal active layer (AL) suitable for water separation processes must show high levels of water permeability, while at the same time being able to reject a wide range of solutes and remain resilient during cleaning process. From a theoretical perspective, a model AL of an Aquaporin-based lipidic biomimetic membrane (ABPM) may even remain water impermeable, but only if they allow for adequate incorporation of proteopolymersomes

where the water permits solely incorporated proteins to move through. As a result, the new AL components must be comprehensively researched so as to accommodate the existing requirements and parameters. For instance, an AL featuring homogenous thickness potential may be able to help proteopolymersome integration succeed. POSS (amine linker), TMC (acyl chloride linker), and polyhedral oligomeric silsesquioxane have been surveyed for possible applications when it comes the inclusion of proteopolymersomes in ABPMs. A research study recently outlined how POSS can be integrated as an AL layer component, with the data suggesting that POSS-TMC-layer distinctly showed a layer without valleys and ridges, but with elevated mechanical stability capacity in Polyacrylonitrile (PAN) membranes [61]. This experimental method can offer a potentially improved platform for the incorporation of proteopolymersomes, if compared to the valley and ridge prone *m*-phenyl diamine-Trimesoyl chloride MPD-TMC networks. A schematic overview of this experimental reaction is provided in **Figure 1**.

For the experimental trials, PA layers of POSS + TMC including polymersomes of PB29-PEO16 in the aqueous phase were created. During the experiment, the effects of vesicles on the AL capabilities were carefully assessed so as to serve as the basis for the integration of AQPs. In this instance, polybutadiene-polyethylene oxide PB29-PEO16 was chosen because of its capacity to create significant quantities of stable polymersomes during aqueous phase, if compared to other PB-PEO polymersomes [62]. When it comes to the microfluidic method, proteopolymersomes (AqpZ, PB33-PEO18, with molecular amphiphile-to-protein-ratio (mPAR) 1:100) were implemented. Specifically, PB33-PEO18 created significant quantities of stable polymersomes in aqueous phase and ensured effective AqpZ inclusion as shown by the small-angle X-ray

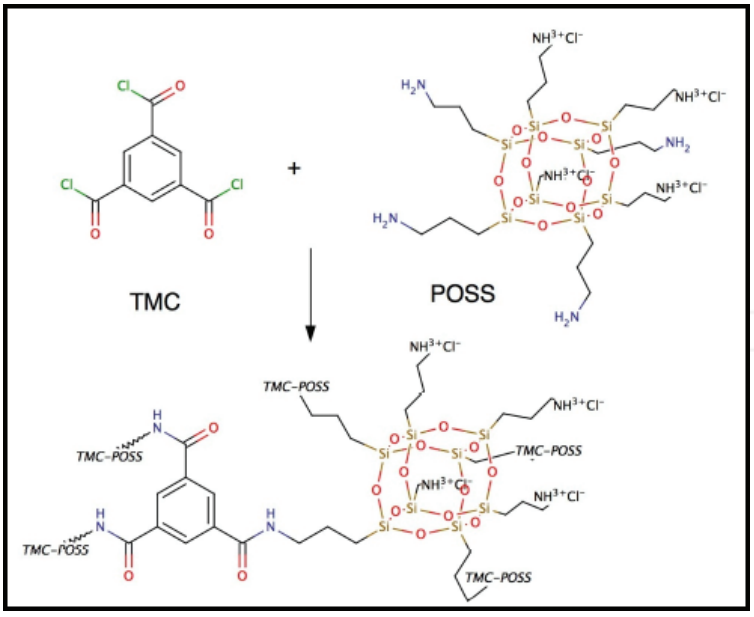

Figure 1. Chemical structure of POSS, TMC, and the resulting AL. POSS acting as the amine linker generates a highly stable and well-defined AL with TMC.

scattering (SAXS). Hexane was introduced as the organic phase, while milli-Q water was used as the aqueous phase. Furthermore, to obtain the smallest possible polydispersity, the polymersomes were sonicated. The process of sonications caused 95% of the polymersomes to show a diameter of 196 ± 83 nm, as the dynamic light scattering (DLS) was able to confirm.

To produce a nonsupported AL, the approach had to add both phases, one after another in a beaker, where an AL supported by microfiltration (MF) polyethersulfone (PES) layers was manufactured with the aid of various coating procedures. Next, the classification of the nonsupported AL was done with SEM, Fourier-transformed infrared spectroscopy (FTIR), and a new microfluidic method that permitted direct observation of the polymerization procedure [63]. For this approach, the characterization of supported AL was accomplished using SEM and FTIR. The supported AL was likewise verified in terms of functionality by implementing rejection and standard flux tests in FO mode and featuring methyl violet staining.

Once both phases are added, the sections of the formed nonsupported AL were first air dried and then effectively vacuum dried. During the process, these sections turned into structures resembling flakes. The FTIR examination of POSS + TMC, with inclusion of polymersomes, showcased the appearance of block copolymers in the AL, and this is visible in **Figure 2**. Specifically, the AL with polymersomes featured an absorption capacity peak at about 3000 cm^{-1} (C—H stretch), and this peak was likewise identified in spectra of PEO and PB [64, 65]. The data reflect that the polymersome-free AL displayed a broader peak at the similar wavelength value range; however, it did not allow for a specific maximum value as was seen in the polymersome-containing AL. These research data may be suggestive of an effective polymersome incorporation occurring in the AL. Moreover, polymersomes did not appear to prevent the PA creation, primarily due to the peaks of a PA bond, the C═O stretch

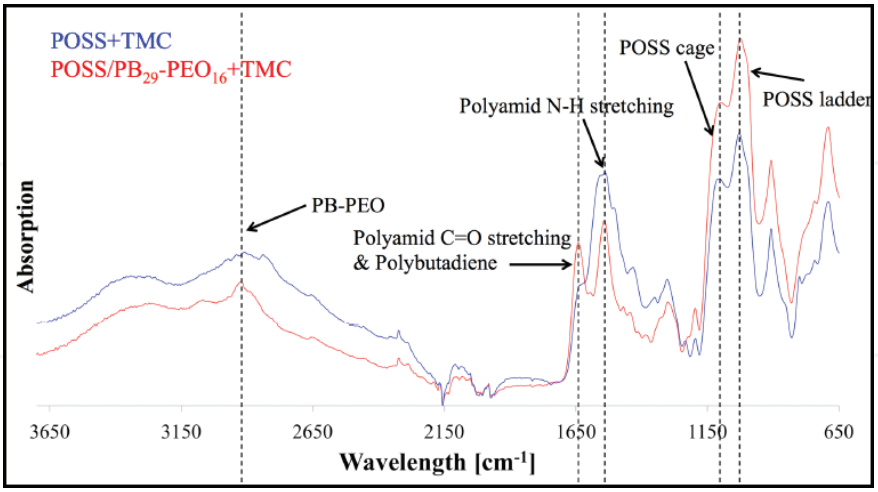

Figure 2. FTIR diagram of POSS/polymersomes + TMC AL (labeled red) and POSS + TMC control AL (labeled blue), as a function of wavelength mapped against absorption values. The AL with polymersomes had an absorption peak around 3000 cm^{-1}. This corresponds to PB and PEO and indicates their presence in the AL, where the characteristic absorption peaks for PA bonds and POSS were likewise present.

at 1636 cm^{-1} and the N—H stretch at 1545 cm^{-1} [61], being openly observable in the AL with polymersomes. Finally, partial hydrolysis of the POSS leading to the AL creation is not seriously disturbed by the occurrence of the polymersomes, as the usual peaks for the POSS-cage and ladder (1125 and 1040 cm^{-1} [61]) were observable in both of the AL. However, there was a noticeable influence of polymersomes on the TMC and its potential reactivity. Initially, Dalwani et al. research collaborative employed 2-g/L TMC for the supported as well as non-supported AL [61]. During the testing, an alternative dynamic was observed where there was a nonsupported AL with 2 g/L, but with 0.5 g/L, TMC could not be incited to form. In theory, the TMC-POSS-stoichiometry was increased artificially due to the existence of other species in the aqueous phase. A surplus amount of TMC can delay the process of network structure construction, as TMC may not be able to connect the POSS cages and developing only in low molecular weight networks. In this case, 0.5-g/L TMC for the POSS/polymersomes + TMC AL and the nonsupported POSS + TMC AL was implemented.

Research data outlined in **Figure 3** show the FTIR outcomes supplemented by an SEM analysis of those samples. The fact that the POSS + TMC AL was seen as well-defined and smooth suggests that the data are in agreement with previously conducted research [61], as can be seen in **Figure 3a** and **b**. Once the polymersomes were introduced (**Figure 3c–e**) to the process, a visible discrepancy could be seen between the sides toward the organic phase. In particular, one of the sides does not show polymersomes presence (**Figure 3c**), while another side facing the aqueous layer is sufficiently coated with polymersomes (**Figure 3e**). The majority of polymersomes present seemed to be loosely stationed on the top AL. On the other hand, some of the polymersomes appeared to be enclosed by the AL at least to a certain, and their overall shape was much less sharp than the other types of shapes, as is shown by the dotted circles within the image in **Figure 3d**. A number of polymersomes were also implanted directly inside the AL, which can be observed when looking at the AL's cracked profile outline (shown by arrows in **Figure 3d**). This dynamic may indicate that the POSS method could be used for embedding the polymersomes in a manner that would make them helpful during the membrane fabrication process. A method based on the microfluidic field was recently published in a research study [63]. This particular approach suggests performing a visual type study of the exact evolution of interfacial polymerization reactions locations. During this assessment, the chip containing a hydrophobized microchamber becomes separated into two compartments with the aid of micropillars, each with a height of 50 μm and a diameter of 30 μm. In this case, the aqueous phase featuring amine linker was initiated using the microcapillary connections into one compartment and then created a water-air interface between the pillars. For the following step, the organic phase including the acyl chloride linker was inserted into the other compartment. The process showed that the AL formation occurring at the point of interface between the present solutions was seen with the aid of an optical microscope. The AL created as a result had a different formation time and morphology, since the parameters depend on the specific linkers. A practical application of this method indicates that the POSS + TMC creates a well-defined AL and has a formation time of within 4 seconds. Alternatively, the visible development of film in Jeffamine + TMC does not finalize even after 15 minutes, and the film itself exhibits the valley and ridge structural dynamic characteristic of AL created using interfacial polymerization [63].

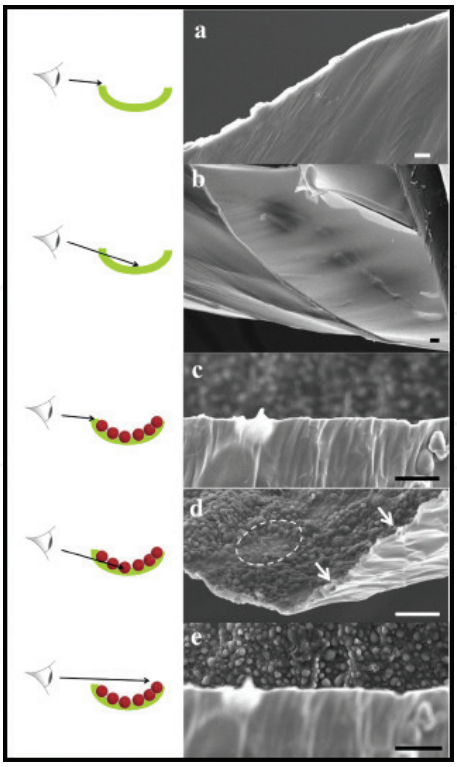

Figure 3. SEM images of POSS + TMC AL (a, b) and POSS/polymersomes + TMC AL (c–e) with schematic sketches, including the part of the layer that is being captured. Images of different flake parts were taken (labeled green in the sketch) for the AL test cases generated during the SEM preparation. The AL without polymersomes was smooth and well-defined and remained on the organic side once polymersomes were added. The aqueous side was covered with loosely attached and half-covered polymersomes (dotted circle in (d)). A few polymersomes could be observed inside the AL (arrows in (d)). Scale bar is 3 μm.

The following method was used to supervise POSS/proteopolymersomes + TMC AL (AqpZ & PB33-PEO18, mPAR 1:100) as shown in **Figure 4**. During the application of this approach, the chip used was not hydrophobized in an optimal manner and as a consequence forced a partial infusion of the aqueous phase directly into the channel space where the organic phase was occurring. However, the hydrophobization process remained sufficiently effective and was able to prevent the aqueous phase from transitioning into the other section in its entirety. Another possible explanation for the interface shift occurring from the pillar structures into the organic phase may be connected to the overpressure dynamic in the aqueous phase, since it is very difficult to regulate when the pressure range is around 104 Pa. The characteristic sharp AL was created on the aqueous-organic interface, once the organic phase containing TMC was introduced (shown in **Figure 4b** using dotted line 1). After this, the reaction proceeded as the diffused amine was added into the organic phase, while the created AL connecting the initial interfaces began to show the appearance of a new aqueous-organic interface

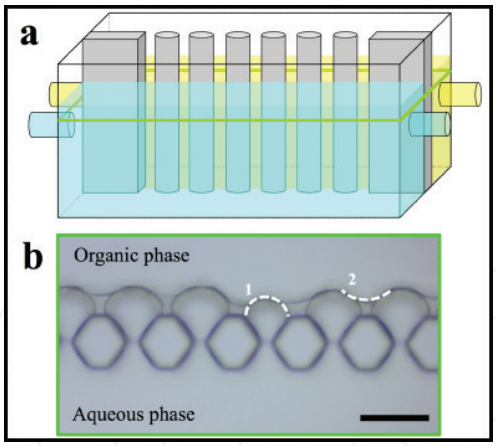

Figure 4. (a) Schematic sketch of the microfluidic chamber and micrographs of POSS/proteopolymersomes + TMC AL and (b) micrograph of the compartment. The aqueous phase entered into the other compartment. After introducing the organic phase, a well-defined AL was formed. The scale bar is 50 μm.

(indicated in **Figure 4b** using dotted line 2). The project's research data and subsequent observations suggest that a less dense AL was created by POSS/proteopolymersomes-TMC than the one created during the POSS-TMC reaction process. In this experimental setup, the formation time value was within the matter of seconds. Evidence likewise showed that the film quality continued to be acceptable and maintained the same shape, without any additional growth noted during the 12 hours that followed.

The POSS + TMC on MF PES support material coating was researched in response to the data produced by Dalwani et al. [61]. In this instance, the MF PES was supported by a nonwoven type of coating. The FTIR spectroscopy testing indicated that the polymersomes were present in the supported AL; on the other hand, the PA formation was substantially lower if compared to the nonsupported POSS/polymersomes + TMC AL, as seen in **Figure 5**. The primary issue that can hinder the analysis of this type of supported AL with FTIR is the possible absorption of the PES support, since it has a significant absorption possibility, specifically, in the sections located between 700 and 2000 cm^{-1}. In fact, the POSS absorption peaks can greatly interfere with the appearing PES peaks. For the supported POSS/polymersomes + TMC AL, a PB-PEO signal was apparent at 3000 cm^{-1}, and another minor peak around 1700 cm^{-1} also appeared in the FTIR spectra of PB [64]. In the case of nonsupported AL, however, peaks could not be identified. From a theoretical standpoint, the reason for this discrepancy is that it was overlayed because of the background signal within the 1600–3650 cm^{-1} region and that was more overpowering during the FTIR analysis spectra for the nonsupported AL. Furthermore, both the PA bonds were noted in the supported POSS + TMC AL, even though they were significantly smaller in the one including polymersomes. Specifically, the large peak (at 1580 cm^{-1}) near the N—H stretching peak is related to PES. The N—H stretching peak (1545 cm^{-1}) occurred solely in the supported POSS + TMC AL. Finally, the broad AL peak located in the range of 3150–3650 cm^{-1} is potentially connected to water and the unreacted amine groups.

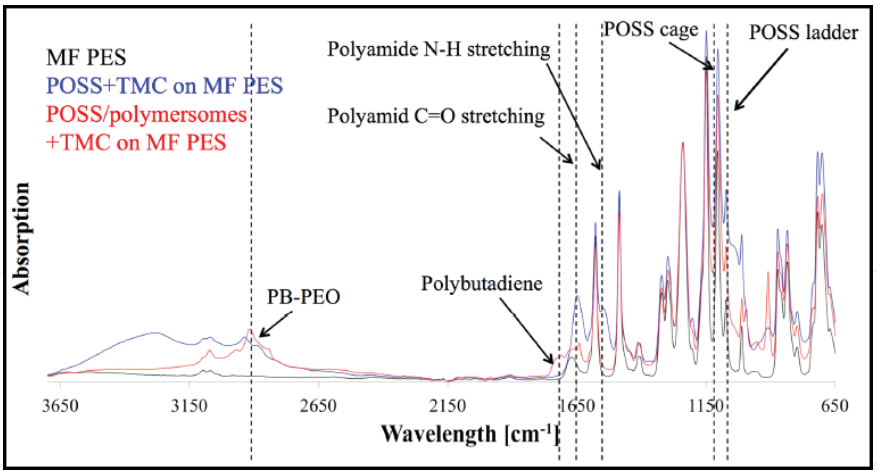

Figure 5. FTIR analysis of supported POSS/polymersomes + TMC AL (**red**) and POSS + TMC control AL (**blue**) on MF PES and pure MF PES (**black**). The PES-supporting material had high absorption values and interfered with numerous absorption peaks. A subtraction from the absorption spectra of pure PES resulted in negative peaks. As a result, only the spectra were normalized. PB-PEO was present in the AL with polymersomes; however, the PA formation was strongly suppressed.

Research data cannot with certainty provide the explanation for the subdual of the PA-signal in the supported POSS/polymersomes + TMC AL. There is a possibility that it might be connected to the TMC and its reactivity potential, a dynamic that has been overviewed earlier. In this experimental approach, 2 g/L TMC for the supported POSS + TMC AL as well as POSS/polymersomes + TMC AL were implemented, since there was no AL creation at 0.5 g/L value. Admittedly, an alternative TMC concentration value might prove to be more ideal for the supported POSS/polymersomes + TMC AL during the applications. Although the blockage of the PA formation incited by polymersomes was supposed to suppress the PA formation in the nonsupported AL, it was not able to do so. With the supported POSS + TMC AL, the AL formation was substantially lowered when altering from 2 to 0.5 g/L. A different hypothesis suggests that POSS + TMC do not in fact form effortlessly on MF PES. Recent research available on this has reported no former POSS + TMC AL formation on MF PES. Since the MF PES has considerably larger pore sizes than PAN, this may effectually impede the creation of a smooth type of layer. In comparison with the FTIR investigation, the SEM analysis revealed a totally covered POSS/polymersomes + TMC AL on the MF PES (shown in **Figure 6**). Moreover, TMC and POSS were able to cover the microporous PES structure in its entirety with a smooth surface layer, even though less distinct than found in PAN substrates [61]. Most likely, this can be attributed to the varying range of pore sizes as reported earlier. The addition of polymersomes facilitated a change and the AL began to exhibit submicron-sized bumps, 0.5–1 μm in height and 1.5–2 μm in length. In this case, with the 100 nm thickness covering AL [61] (**Figure 6** sketch in bottom left corner), there would appear to be groups of 6–9 polymersomes in a row with 1–3 layers. Unlike the nonsupported ALs arrangement, in this instance, only the side facing the organic phase can be effectually observed. When it

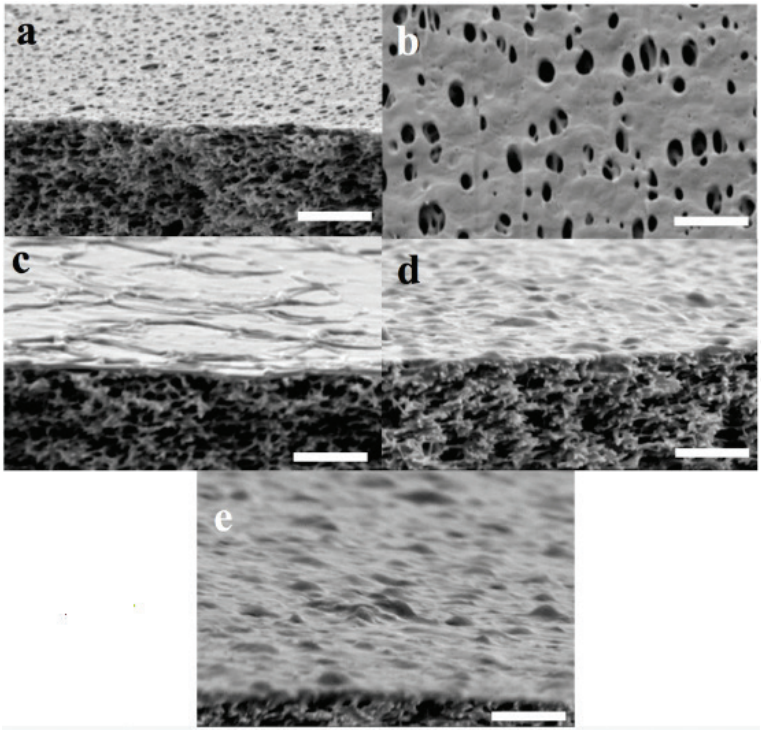

Figure 6. SEM images of MF PES (a, b) supported POSS + TMC AL on MF PES (c) and supported POSS/polymersomes+TMC on MF PES (d, e). Schematic sketch of polymersome coverage on the left (e). Micropores of the MF PES were covered completely by the POSS + TMC AL. After the addition of polymersomes, small bumps with dimensions similar to the polymersomes were observed on the side facing the organic in the AL. Greater bumps may be attributed to the accumulation of covered polymersomes. Scale bar is 3 μm.

comes to the supported POSS/polymersomes + TMC AL, polymersomes have a significantly greater effect on the shape of the AL side facing the organic phase than in examples with the nonsupported forms. Mostly this is caused by the variance in preparation and specifically with respect to POSS/polymersomes in solution at the nonsupported AL formation, occurring at the water-air interface or even being dried up on the MF PES at the supported AL formation. As a consequence, the overall probability of polymersomes being incorporated in the AL is greater for the supported AL rather than the nonsupported AL.

To conclude, the SEM analysis helped to successfully show the incorporation of polymersomes into a supported AL, even though the FTIR research information was potentially less reflexive of its internal dynamics and processes. The issue that limits the SEM and FTIR interrogation of the supported AL is that only a minor portion of the whole membrane is actually observed. Other concerns that can negatively affect a more in-depth study is that the AL samples can become brittle during the process of drying and then delaminate or possibly break off when exposed to liquid nitrogen currently being used for SEM sample preparation.

The new experimental directions included testing of POSS/polymersomes + TMC AL on MF PES with respect to flux potential and rejection values with FO mode. Notably, the collected data showed a lack of FO performance. An estimated one third of the membranes experimentally tested were determined to be impermeable to salt, as indicated by the small conductivity change occurring in the feed solution after 2 h. The remaining membranes were found to be leaky, which was reflected by an instant conductivity growth. Furthermore, only a minor fraction of the POSS/polymersomes + TMC and POSS + TMC leaky and sealed membranes could be assessed as comparable. Within the sealed type membranes, the pores were most likely obstructed by multiple collected layers of POSS + TMC AL. Moreover, the process of methyl blue staining showed an absence of scratches and pinholes on the surface, further indicating that the supporting PES was entirely covered with the AL. As research testing has already illustrated, MF PES is not capable of providing adequate general support for POSS + TMC ALs. Due to the smaller pore size between 5 and 30 nm, PAN support did not exhibit any flux without the added hydraulic pressure [66]. Such a dynamic may be suitable for POSS + TMC with a NF membrane; however, it is not sufficient for the FO. Research approach published by Lee et al. offers a potential compromise that would be based on employing UF PES membranes [67].

This subchapter focused on new insights with regard to the supported and nonsupported AL including POSS with polymersomes during the aqueous phase and TMC during the organic phase. The experimental runs showed that the nonsupported POSS/polymersomes + TMC AL could be successfully developed, with large number of polymersomes coated and a smaller number of them incorporated inside the AL. In particular, the supported POSS/polymersomes + TMC displayed a range of relevant properties. While the FTIR suggested a high suppression potential of the AL formations in cases where polymersomes were added, the SEM images indicated an entirely coated and substantially different AL after the addition of polymersomes. Experimental data showed that none of the created membranes that included TMC and POSS provided successful performances, most likely because of the incomplete coverage of the AL. Even though the experimental results were limited, the exploration of this approach was essential for future development of insight into how proteopolymersomes, TMC, and POSS are engaging with each other. There is a need to explore new avenues of research, and the next specific set of challenges will aim to develop a functional and effective water separation membrane based on these components and their potential strengths.

Author details

Amira Abdelrasoul[1]*, Huu Doan[2] and Ali Lohi[2]

*Address all correspondence to: amira.abdelrasoul@usask.ca

1 Department of Chemical and Biological Engineering, University of Saskatchewan, Saskatoon, Saskatchewan, Canada

2 Department of Chemical Engineering, Ryerson University, Toronto, Ontario, Canada

References

[1] Choi HJ, Montemagno C. Recent progress in advanced nanobiological materials for energy and environmental applications. Materials. 2013;**6**:5821-5856

[2] Pendergast MM, Hoek EMV. A review of water treatment membrane nanotechnologies. Energy & Environmental Science. 2011;**4**:1946-1971

[3] Ishibashi K. Aquaporin subfamily with unusual NPA boxes. Biochimica et Biophysica Acta. 2006;**1758**:989-993

[4] Verkman AS. More than just water channels: Unexpected cellular roles of aquaporins. Journal of Cell Science. 2005;**118**:3225-3232

[5] Montemagno C, Schmidt J, Tozzi S. Biomimetic Membranes. Patent WO 2004/011600; 5 February 2004

[6] Hansen JS, Perry M, Vogel J, Vissing T, Hansen CR, Geschke O, Emnéus J, Hélix-Nielsen C. Development of an automation technique for the establishment of functional lipid bilayer arrays. Journal of Micromechanics and Microengineering. 2009;**19**:2. DOI: 10.1088/0960-1317/19/2/025014

[7] Hansen JS. Development of supported biomimetic membranes for insertion of aquaporin protein water channels for novel water filtration applications. [Ph.D. thesis], Danish Technical University, Kgs. Lyngby: Denmark; 2010

[8] Pszon-Bartosz K, Hansen JS, Stibius KB, Groth JS, Emnéus J, Geschke O, Hélix-Nielsen C. Assessing the efficacy of vesicle fusion with planar membrane arrays using a mitochondrial porin as reporter. Biochemical and Biophysical Research Communications. 2011;**406**:96-100

[9] González-Pérez A, Stibius K, Vissing T. Biomimetic triblock copolymer membrane arrays: A stable template for functional membrane proteins. Langmuir. 2009;**25**:10447-10450

[10] Rein C, Pszon-Bartosz K, Stibius KB, Bjørnholm T, Hélix-Nielsen C. Free-standing biomimetic polymer membrane imaged with atomic force microscopy. Langmuir. 2011;**27**: 499-503

[11] Ibragimova S, Stibius K, Szewczykowski P, Perry M, Bohr H, Hélix-Nielsen C. Hydrogels for in situ encapsulation of biomimetic membrane arrays. Polymers for Advanced Technologies. 2010;**23**:182-189

[12] Perry M, Hansenz J, Stibius K. Surface modifications of support partitions for stabilizing biomimetic membrane arrays. Journal of Membrane Science and Technology. 2011. DOI: 10.4172/2155-9589.S1-001

[13] Rein C. Stabilization and characterization of 2D and 3D biomimetic membranes. [Ph.D. thesis], University of Copenhagen; Copenhagen, Denmark, 2011

[14] Aquaporin A/S. Biomimetic Membranes and Uses Thereof. Patent WO 2010/146365, 23 December 2010

[15] Aquaporin A/S. Membrane for Filtering of Water. Patent WO 2006/122566; 23 November 2006

[16] Aquaporin A/S. Biomimetic Water Membrane Comprising Aquaporins Used in the Production of Salinity Power. Patent WO 2007/033675; 29 March 2007

[17] Aquaporin A/S. Scaffold for Composite Biomimetic Membrane. Patent WO 2009/074155; 18 June 2009

[18] Aquaporin A/S. Assays Relating to Biomimetic Membranes and Their Uses. Patent WO 2010/146366; 23 December 2010

[19] Mech-Dorosz A, Heiskanen A, Bäckström S, Perry M, Muhammad HB, Hélix-Nielsen C, Emnéus J. A reusable device for electrochemical applications of hydrogel supported black lipid membranes. Biomedical Microdevices. 2015;**17**:21

[20] Montemagno C, Aquaz, Danfoss. Nanofabricated Membrane Using Polymerized Proteoliposomes. Patent WO 2010/091078, 12 August 2010

[21] Wang H, Chung TS, Tong YW, Meier W, Chen Z, Hong M, Jeyaseelan K, Armugam A. Preparation and characterization of pore-suspending biomimetic membranes embedded with aquaporin Z on carboxylated polyethylene glycol polymer cushion. Soft Matter. 2011;**7**:7274

[22] Kumar M. Biomimetic membranes as new materials for applications in environmental engineering and biology. [Ph.D. thesis], University Illinois: Champaign, IL USA; 2010

[23] Sun G, Zhou H, Li Y, Jeyaseelan K, Armugam A, Chung TS. A novel method of AquaporinZ incorporation via binary-lipid Langmuir monolayers. Colloids and Surfaces B: Biointerfaces. 2012;**89**:283-288

[24] Kaufman Y, Grinberg S, Linder C, Heldman E, Gilron J, Freger V. Fusion of Bolaamphiphile micelles: A method to prepare stable supported biomimetic membranes. Langmuir. 2013;**29**:1152-1161

[25] Li X, Wang R, Wicaksana F, Zhao Y, Tang CY, Torres J, Fane AG. Fusion behaviour of aquaporin Z incorporated proteoliposomes investigated by quartz crystal microbalance with dissipation (QCM-D). Colloids and Surfaces B: Biointerfaces. 2013;**111**:446-452

[26] Kaufman Y, Berman A. Supported lipid bilayer membranes for water purification by reverse osmosis. Langmuir. 2010;**26**:7388-7395

[27] Freger V, Kaufman Y. Biomimetic Membranes, Their Production and Uses Thereof in Water Purification. Patent US 2011/0084026; 14 April 2011

[28] Li X, Wang R, Tang CY, Vararattanavech A, Zhao Y, Torres J, Fane AG. Preparation of supported lipid membranes for aquaporin Z incorporation. Colloids and Surfaces B: Biointerfaces. 2012;**94**:333-340

[29] Zhao Y, Qiu C, Li X, Vararattanavech A, Shen W, Torres J, Hélix-Nielsen C, Wang R, Hu X, Fane AG, et al. Synthesis of robust and high-performance aquaporin-based biomimetic membranes by interfacial polymerization-membrane preparation and RO performance characterization. Journal of Membrane Science. 2012;**423-424**:422-428

[30] Aquaporin AS. NTU. Aquaporin Based Thin Film Composite Membranes. Patent WO 2013/043118; 28 March 2013

[31] Aquaporin AS. Systems for Water Extraction. Patent WO 2014/128293; 28 August 2014

[32] Zhao Y, Vararattanavech A, Li X, Hélix-Nielsen C, Vissing T, Torres J, Wang R, Fane AG, Tang CY. Effects of Proteoliposome composition and draw solution types on separation performance of aquaporin-based Proteoliposomes: Implications for seawater desalination using aquaporin-based biomimetic membranes. Environmental Science & Technology. 2013;**5**:1496-1503

[33] Li X, Wang R, Wicaksana F, Tang CY, Torres J, Fane AG. Preparation of high performance nanofiltration (NF) membranes incorporated with aquaporin Z. Journal of Membrane Science. 2014;**450**:181-188

[34] Tanner P. Design and development of protein-polymer assemblies to engineer artificial organelles. [Ph.D. thesis], Universität Basel: Basel, Switzerland; 2013

[35] Pawar PV, Gohil SV, Jain JP, Kumar N. Functionalized polymersomes for biomedical applications. Polymer Chemistry. 2013;**4**:3160-3176

[36] Jesorka A, Orwar O. Liposomes: Technologies and analytical applications. Annual Review of Analytical Chemistry. 2008;**1**:801-832

[37] Montemagno C. Biomimetic Membrane Formed from a Vesicle-Thread Conjugate. Patent WO 2010/040353, 15 April 2010

[38] Wang H, Chung TS, Tong YW, Jeyaseelan K, Armugam A, Chen Z, Hong M, Meier W. Highly permeable and selective pore-spanning biomimetic membrane embedded with aquaporin Z. Small. 2012;**8**:1185-1190

[39] Kumar M, Grzelakowski M, Zilles J, Meier WP. Highly permeable polymeric membranes based on the incorporation of the functional water channel protein aquaporin Z. Proceedings of the National Academy of Sciences of the United States. 2007;**104**: 20719-20724

[40] Zhong PS, Chung TS, Jeyaseelan K, Armugam A. Aquaporin-embedded biomimetic membranes for nanofiltration. Journal of Membrane Science. 2012;**407-408**:27-33

[41] Duong PHH, Chung TS, Jeyaseelan K, Armugam A, Chen Z, Yang J, Hong M. Planar biomimetic aquaporin-incorporated triblock copolymer membranes on porous alumina supports for nanofiltration. Journal of Membrane Science. 2012;**409-410**:34-43

[42] Wang HL, Chung TS, Tong YW, Jeyaseelan K, Armugam A, Duong HHP, Fu F, Seah H, Yang J, Hong M. Mechanically robust and highly permeable AquaporinZ biomimetic membranes. Journal of Membrane Science. 2013;**434**:130-136

[43] Wang H, Chung TS, Tong YW. Study on water transport through a mechanically robust aquaporin Z biomimetic membrane. Journal of Membrane Science. 2013;**445**:47-52

[44] Xie W, He F, Wang B, Chung TS, Jeyaseelan K, Armugam A, Tong YW. An aquaporin-based vesicle-embedded polymeric membrane for low energy water filtration. Journal of Materials Chemistry A. 2013;**1**:7592-7600

[45] Sun G, Chung TS, Jeyaseelan K, Armugam A. Stabilization and immobilization of aquaporin reconstituted lipid vesicles for water purification. Colloids and Surfaces B: Biointerfaces. 2012;**102**:466-471

[46] Kaufman Y, Grinberg S, Linder C, Heldman E, Gilron J, Shen YX, Kumar M, Lammertink RGH, Freger V. Towards supported bolaamphiphile membranes for water filtration: Roles of lipid and substrate. Journal of Membrane Science. 2014;**457**:50-61

[47] Sun G, Chung TS, Jeyaseelan K, Armugam A. A layer-by-layer self-assembly approach to developing an aquaporin-embedded mixed matrix membrane. RSC Advances. 2013;**3**:473

[48] Sun G, Chung TS, Chen N, Lu X, Zhao Q. Highly permeable aquaporin-embedded biomimetic membranes featuring a magnetic-aided approach. RSC Advances. 2013;**3**:9178-9184

[49] Wang M, Wang Z, Wang X, Wang S, Ding W, Gao C. Layer-by-layer assembly of aquaporin Z-incorporated biomimetic membranes for water purification. Environmental Science & Technology. 2015;**49**:3761-3768

[50] Shen YX, Saboe PO, Sines IT, Erbakan M, Kumar M. Biomimetic membranes: A review. Journal of Membrane Science. 2014;**454**:359-381

[51] Thomas JA, McGaughey AJH. Reassessing fast water transport through carbon nanotubes. Nano Letters. 2008;**8**:2788-2793

[52] Holt J, Park H, Wang Y, Stadermann M, Artyukhin A, Grigoropoulos C, Noy A, Bakajin O. Fast mass transport through Sub-2-Nanometer carbon nanotubes. Science. 2006;**312**:1034-1037

[53] Fei Z, Zhao D, Geldbach TJ, Scopelliti R, Dyson PJ, Antonijevic S, Bodenhausen G. A synthetic zwitterionic water channel: Characterization in the solid state by X-ray crystallography and NMR spectroscopy. Angewandte Chemie, International Edition. 2005;**44**:5720-5725

[54] Barboiu M. Artificial water channels. Angewandte Chemie, International Edition. 2012;**51**:11674-11676

[55] Percec V, Dulcey AE, Balagurusamy VSK, Miura Y, Smidrkal J, Peterca M, Nummelin S, Edlund U, Hudson SD, Heiney PA, Duan H, Magonov SN, Vinogradov SA. Self-assembly of amphiphilic dendritic dipeptides into helical pores. Nature. 2004;**430**:764-768

[56] Zhou X, Liu G, Yamato K, Shen Y, Cheng R, Wei X, Bai W, Gao Y, Li H, Liu Y, et al. Self-assembling subnanometer pores with unusual mass-transport properties. Nature Communications. 2012;**3**. DOI: 10.1038/ncomms1949

[57] Tang CY, Zhao Y, Wang R, Hélix-Nielsen C, Fane AG. Desalination by biomimetic aquaporin membranes: Review of status and prospects. Desalination. 2013;**308**:34-40

[58] Alsvik I, Hägg MB. Pressure retarded osmosis and forward osmosis membranes: Materials and methods. Polymer. 2013;**5**:303-327

[59] Wittbecker EL, Morgan PW. Interfacial polycondensation. I. Journal of Polymer Science. 1959;**40**:289-297

[60] Ghosh AK, Jeong BH, Huang X, Hoek EMV. Impacts of reaction and curing conditions on polyamide composite reverse osmosis membrane properties. Journal of Membrane Science. 2008;**311**:34-45

[61] Dalwani M, Zheng J, Hempenius M, Raaijmakers MJT, Doherty CM, Hill AJ, Wessling M, Benes NE. Ultra-thin hybrid polyhedral silsesquioxane-polyamide films with potentially unlimited 2D dimensions. Journal of Materials Chemistry. 2012;**22**(30):14835-14838

[62] Zawada JF, Yin G, Steiner AR, Yang J, Naresh A, Roy SM, Gold DS, DS HHG, Murray CJ. Microscale to manufacturing scale-up of cell-free cytokine production—A new approach for shortening protein production development timelines. Biotechnology and Bioengineering. 2011;**108**:1570-1578

[63] Zhang Y, Benes NE, Lammertink RGH. Visualization and characterization of interfacial polymerization layer formation. Lab on a Chip. 2015;**15**:575-580

[64] Plasencia I, Survery S, Ibragimova S, Hansen JS, Kjellbom P, Helix-Nielsen C, Johanson U, Mouritsen OG. Structure and stability of the spinach aquaporin SoPIP2;1 in detergent micelles and lipid membranes. PLoS One. 2011;**6**:e14674

[65] Andersen OS, Nielsen C, Maer AM, Lundbæk JA, Goulian M, Koeppe RE II. Gramicidin channels as molecular force transducers in lipid bilayers. Biol. Skr. Dan. Vid. Selsk. 1998;**49**:75-82

[66] Germic L, Ebert K, Bouma RHB, Borneman Z, Mulder MHV, Strathmann H. Characterization of polyacrylonitrile ultrafiltration membranes. Journal of Membrane Science. 1997;**132**:131-145

[67] Lee KP, Zheng J, Bargeman G, Kemperman AJB, Benes NE. pH stable thin film composite polyamine nanofiltration membranes by interfacial polymerisation. Journal of Membrane Science. 2015;**478**:75-84